

December 2019
Version 1.0

Global Hyperspectral Imaging Spectral-library of Agricultural crops (GHISA)
Area of Study: Central Asia

Algorithm Theoretical Basis Document (ATBD)
USGS EROS
Sioux Falls, South Dakota

USGS EROS
Sioux Falls, South Dakota

Document history

| Document Version | Publication Date | Description |
|------------------|------------------|-------------|
| 1.0 | | Original |
| | | |
| | | |
| | | |

| | |
|---|-----------|
| Contents | |
| Document history | 2 |
| I. Members of the team | 2 |
| II. Historical context and background information | 2 |
| III. Hyperspectral input data: EO-1 Hyperion and ASD Spectroradiometer | 4 |
| IV. Algorithm description and Data processing | 7 |
| 1. Algorithms..... | 6 |
| 1.1 Algorithms details | 6 |
| a. Image pre-processing and spectral library..... | 8 |
| b. Algorithms for selection of optimal wavebands to detect crop types | 9 |
| 1.2 Programming and code | 10 |
| 2. Results | 11 |
| a. Spectral Library..... | 11 |
| b. Algorithms for Selection of Optimal Wavebands that Detect Crop Types..... | 12 |
| V. Constraints and limitations | 17 |
| VI. Conclusions | 17 |
| VII. Publications | 17 |
| VIII. Acknowledgements | 17 |
| IX. Contact information | 18 |
| X. Citations | 18 |
| XI. References | 18 |

I. Members of the team

The Global Hyperspectral Imaging Spectral-library of Agricultural crops (GHISA) for Central Asia was produced by the following team members. Their specific role is mentioned below.

Dr. Isabella Mariotto, CEO and Geospatial Scientist, Terra Sensing Lab, LLC, and former Postdoctoral Research Scientist, USGS, with guidance from Dr. Thenkabail preprocessed and processed Hyperion images in ENVI and ArcGIS, extracted spectra from the images, developed algorithms in SAS to select optimal wavebands to detect crop types, and compiled GHISA for Central Asia. She also made significant contribution in writing the ATBD and User Guide for Central Asia.

Dr. Prasad S. Thenkabail, Research Geographer, United States Geological Survey (USGS), is the Principal Investigator (PI) of the GHISA project. Dr. Thenkabail was instrumental in developing the conceptual framework of the project and the product. He made significant contribution in writing the manuscript, Algorithm Theoretical Basis Document (ATBD), User Guide, and providing scientific guidance on the GHISA project.

Dr. Itiya P. Aneece, Postdoctoral Research Geographer, USGS, with guidance from Dr. Thenkabail, preprocessed Hyperion images in Google Earth Engine, extracted spectra from the images, and compiled GHISA for the conterminous United States. She also contributed to the manuscript, ATBD, and User Guide.

II. Historical context, background, and need for GHISA

Aneece and Thenkabail (2019a and 2019b) provided the overall context and overview of the global hyperspectral imaging spectral library of agricultural crops (GHISA) as follows:

“Agricultural crop characterization, modeling, mapping, and monitoring are crucial for accurately assessing crop traits, yields, and productivity (e.g., crop productivity, crop water productivity) which in turn helps in assessing and managing global food and water security. Since agricultural crops consume 80-90% of all human water use (Thenkabail et al., 2012, 2010), accurate cropland studies contribute to accurate water use assessments and crop water productivity assessments. Agricultural crop signatures greatly vary by crop type, growth stage, growing condition, management, soil type, climate, and a host of other factors (e.g., inputs like nitrogen, potassium, and phosphorous; pests, and diseases).

Agricultural characteristics and traits can be well established using hyperspectral data that are acquired with clear and precise knowledge of various crop variables. Any such study requires us to gather hyperspectral libraries of crops taking into consideration all factors mentioned above. Vegetation or agricultural crop hyperspectral data are widely used in research as detailed in the new four-volume book-set on hyperspectral remote sensing of vegetation (Thenkabail et al. 2018 a, b, c, d) as well as numerous research papers (Oliphant et al. 2019, Teluguntla et al. 2018, Gumma et al. 2018, Aneece and Thenkabail 2018, Marshall et al. 2014, Mariotto et al. 2013, Thenkabail et al. 2013). These data are collected from various platforms (Ortenberg, 2018, Hoque and Phinn, 2018). Spaceborne sensors include the recently decommissioned United States of America’s (USA) Earth Observing-1 (EO-1) Hyperion (Aneece et al. 2018, Moharana and Dutta 2016,

Oskouei and Babakan 2016), Germany's Environmental Mapping and Analysis Program (EnMAP) (Bracken et al. 2019, Okujeni et al. 2015), the Italian Compact High Resolution Imaging Spectrometer (CHRIS) onboard of the Project for On Board Autonomy (PROBA) satellite (CHRIS PROBA) (Verrelst et al. 2012, Lin et al. 2019), the German Aerospace Center (German: Deutsches Zentrum für Luft- und Raumfahrt e.V.) or DLR's Earth Sensing Imaging Spectrometer (DESI) (Krutz et al. 2019), and upcoming US NASA's SBG (formerly known as HypIRI; Lee et al. 2015, Iqbal et al. 2018, Clark 2017), and the Japanese Hyperspectral Imager Suite (HISUI) (Matsunaga et al. 2018). Airborne sensors include NASA's Airborne Visible InfraRed Imaging Spectrometer-Next Generation (AVIRIS-NG) (Bhattacharya et al. 2019, Ratheesh et al. 2019, Chaube et al. 2019, Jha et al. 2019), the US Hyperspectral Digital Imagery Collection Experiment (HYDICE) (Zhang et al. 2006), Hyperspectral Sensor Surveying (AISA-EAGLE) (Mansour et al. 2012, Lausch et al. 2015, Abdel-Rahman et al. 2015), hyperspectral imaging sensor (HyMap) (Riaza et al. 2014, Buzzi et al. 2014), Compact Airborne Spectrographic Imager (CASI) (Legleiter et al. 2016, Xu et al. 2018), AisaEAGLET (Doneus et al. 2014), and airborne Portable Remote Imaging SpectroMeter (PRISM) (Thompson et al. 2015, Mourolis et al. 2014). Drone-based sensors include Micro-Hyperspec X sensors (Dao et al. 2019, Guo et al. 2019), Rikola Hyperspectral camera (Ivushkin et al. 2019, Mozgeris et al. 2018), SOC710-GX (Rhee et al. 2018, Adao et al. 2017), Specim ImSpector V10 2/3 (Franceschini et al. 2017, Meij et al. 2017), OCI-UAV-1000 (Cahalane et al. 2017, Manfreda et al. 2018), MicroHSI 410-SHARK (Manfreda et al. 2018), and Pika series by Resonon (Kanning et al. 2018). Ground-based sensors include ASD Field Spec (Salem 2017, Padghan and Deshmukh 2017), Ocean Optic USB4000 (Middleton 2010), and UniSpec DC Spectrometer Analysis System (Davidson et al. 2016), and Spectral Evolution field portable spectroradiometers (Maimaitiyiming et al. 2016).

Hyperspectral data are collected and analyzed for various study sites in the world and the results are shared in reports and research papers. Unfortunately, the hyperspectral libraries of the crops or vegetation used in these papers are either not shared or shared by only a few researchers, often in an uncoordinated manner. Currently, **a systematic Global Hyperspectral Imaging Spectral-library of Agricultural crops (GHISA) does not exist**. The need for a GHISA is of utmost importance in the current scenario of increased availability of advanced hyperspectral sensors on various platforms (Ortenberg 2018, Hoque and Phinn 2018, Ghamisi et al. 2017, Panda et al. 2015). **GHISA is a**

“Comprehensive and systematic collection, collation, synthesis, standardization, and characterization of global agricultural crop hyperspectral signatures obtained from spaceborne, airborne (e.g., aircrafts, drones), platform-mounted, and ground-based hand-held spectroradiometers or imaging spectroscopy. The GHISA data are collected as near continuous spectra (e.g., every 1 or 10 nm) along a range of the electromagnetic spectrum (e.g., 400-2500 nm or 400-1000 nm or 8000-14000 nm). The collection and collation protocols of GHISA data are well defined and documented. GHISA data are processed using a standard set of protocols and algorithms for converting raw data into surface reflectance. Synthesis of GHISA data involves linking them to globally understood crop characteristics such as agroecological zones, precise geolocation, crop types, crop growing conditions, watering methods (e.g., irrigated or rainfed), and numerous other variables (e.g., inputs such as nitrogen applied, genome, etc). GHISA spectral libraries must have large sample sizes for each class to be robust. Characterization of GHISA data

could include, for example, a comparison of hyperspectral narrowband data with multispectral broadband data for every crop type”.

The need is multi-fold to understand, model, map, and monitor the following crop traits and/or help answer the following questions:

1. What are the typical hyperspectral signatures of individual agricultural crops? How do these hyperspectral signatures vary during different: (a) growth stages, (b) geographical area, (c) genomes, (d) management practices, (e) inputs, (f) and a host of other parameters (e.g., irrigation versus rainfed, soils)?
2. How does the same crop that is grown in different parts of the world change in its hyperspectral characteristics? Why?
3. How do hyperspectral signatures of crops acquired over an area for one season compare across years (e.g., during normal, drought, and wet years)?
4. What crop traits can be quantified by GHISA hyperspectral libraries? What are their accuracies?
5. How can technological advances over the years change the ability of the GHISA hyperspectral library to characterize a crop?
6. How do hyperspectral crop characteristics vary from crop to crop?
7. What advances can be made in understanding, modeling, mapping, and monitoring agricultural crops using hyperspectral narrowband data as opposed to multispectral broadband data?
8. What unique hyperspectral vegetation indices (HVIs) are developed that help advance our understanding of agricultural crop characteristics relative to multispectral broadband data derived vegetation indices (MBVIs)? What unique crop characteristics that cannot be characterized by MBVIs are characterized by HVIs?
9. How do the GHISA hyperspectral signatures of a particular crop acquired from different platforms (e.g., spaceborne, airborne, ground-based) compare and/or contrast?
10. How can GHISA help local, regional, federal, and international entities make informed decisions on agricultural practices?
11. How can other scientists voluntarily provide input on individual crops to a GHISA library? Crowd-sourcing spectral data collection might be an interesting off-shoot to pursue.

In a nutshell, GHISA provides a knowledge-bank of agricultural crops of the world grown in different countries, regions, agroecological zones, and conditions. It will serve many purposes of scientific and practical applications. For example, GHISA will be a signature bank for training algorithms for crop type mapping or to establish their quantitative traits to develop crop biophysical and biochemical models (Aneece and Thenkabail, 2018)”.

III. Hyperspectral input data: EO-1 Hyperion and ASD Spectroradiometer

This Algorithm Theoretical Basis Document (ATBD) provides a detailed account of the GHISA product, which is generated using Earth Observing-1 (EO-1) spaceborne hyperspectral Hyperion satellite sensor data. There are 70,000+ EO-1 Hyperion hyperspectral images (Figure 1) acquired over 2000 to 2015 time-frame and available for free from USGS EarthExplorer

(<https://earthexplorer.usgs.gov/>). For the full description of the EO-1 Hyperion data please refer to Barry (2001), Khurshid et al. (2006), and Scheffler and Karrasch (2014).

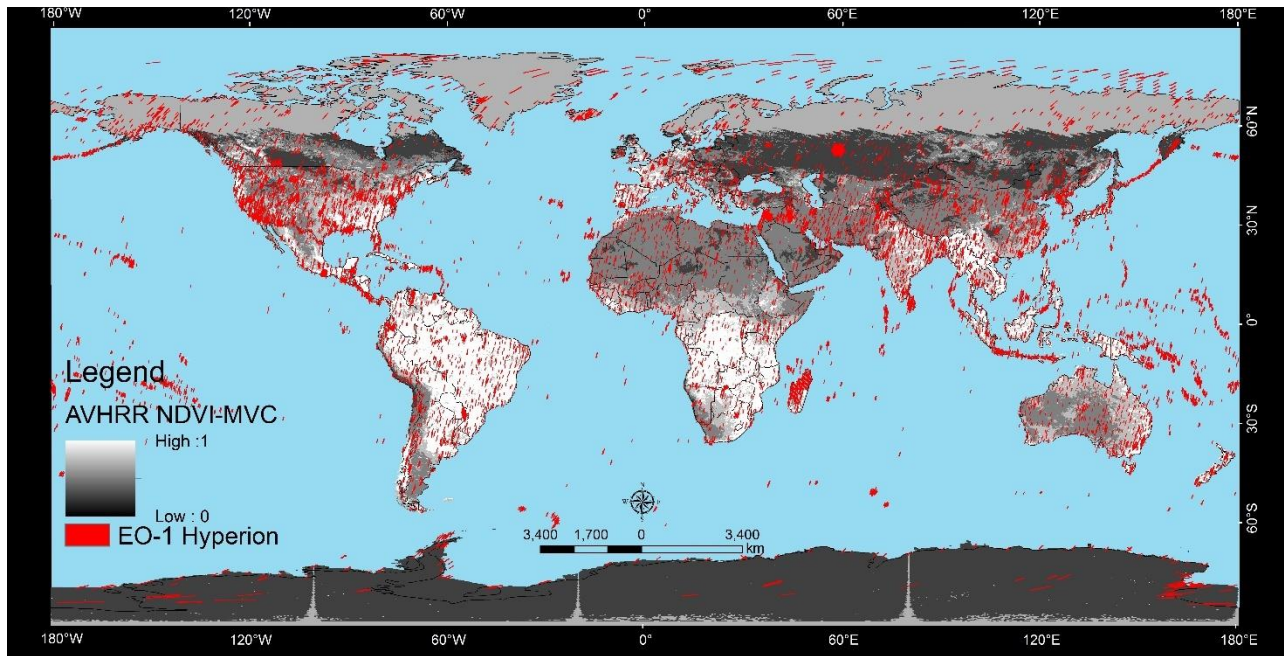


Figure 1. Spaceborne EO-1 Hyperion hyperspectral data acquired over the world from year 2000 to 2015. Over 70,000+ images are available for free download from the USGS EarthExplorer (<https://earthexplorer.usgs.gov/>). Each image is 185 km x 7.5 km and has 242 spectral bands each 10 nanometer wide in 400-2500 nm range (Source: Thenkabail et al., 2012).

This document describes the GHISA production scheme **for Central Asia** based on EO-1 Hyperion and ASD spectroradiometer data acquired in irrigated croplands of the Syr Darya River Basin (SRB) in Uzbekistan over Kuva and Galaba farms (Figure 2). Detailed descriptions of these data are provided in Mariotto et al. (2013) as well as in Thenkabail et al. (2013), Biradar et al. (2009), Cai and Thenkabail (2010) and Cai et al. (2008). There were three EO-1 Hyperion images (Table 1). The two areas were selected based on multiple Hyperion images available for the site as well as availability of five major world crops (wheat, rice, corn, alfalfa, cotton). Hyperion data for the 2007 growing season were selected because Hyperion is the only known source of spaceborne hyperspectral data covering the entire world consistently over long time-periods. Such data will enable a comprehensive and systematic study of the world's agricultural crops over multiple years. Crop biomass discrimination was also studied for all five leading world crops.

Several thousand hyperspectral ASD (Analytical Spectral Devices) Spectroradiometer data were consistently collected for each ground point location for the five crops – wheat, cotton, corn, rice, and alfalfa – (Figure 2) in 59 different days (41 days in 2006 and 18 days in 2007) during the 2006 and 2007 crop growing seasons (Table 1). Crop biomass discrimination was also studied for all five leading world crops.

It is imperative to monitor crops and assess global food security, especially with increasing global populations, urbanization, and changing dietary preferences. Knowledge of crop types and crop

growth stages can help assess crop productivity. Remote sensing can be used to classify vegetation, and hyperspectral remote sensing specifically can enable the differentiation of crop types and crop growth stages.

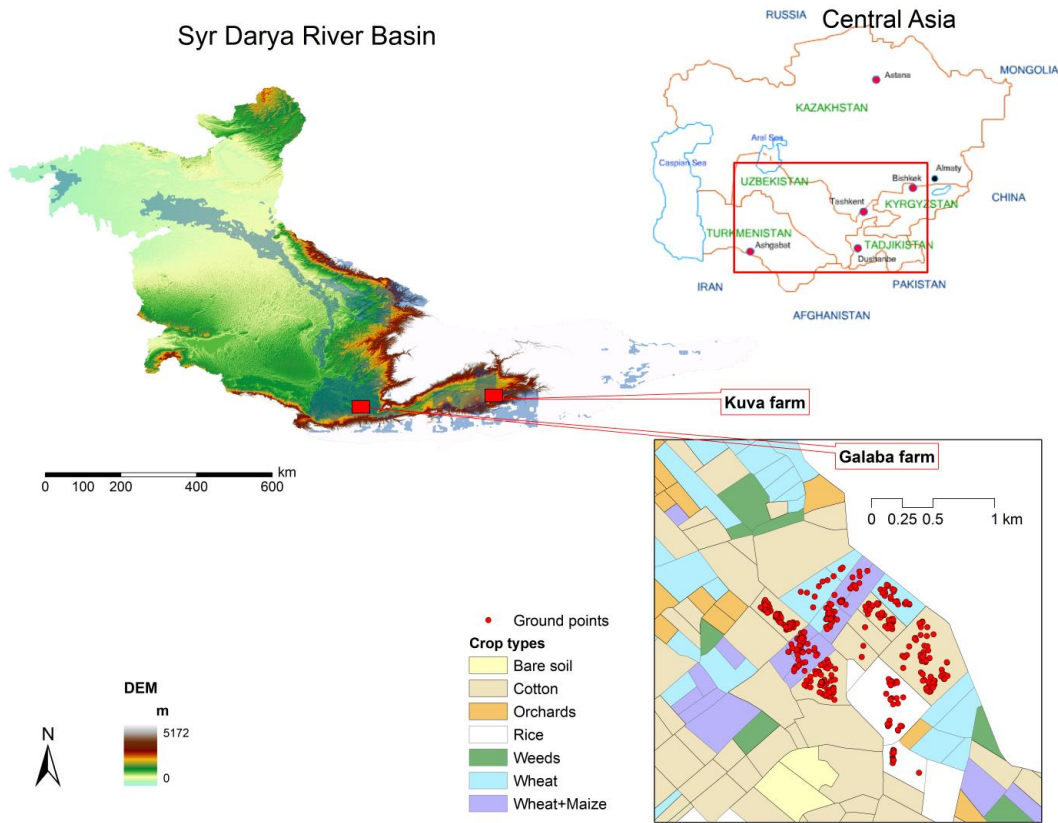


Figure 2. Study area: Galaba and Kuva farm fields in the Syr Darya river basin, Central Asia. Measurements were carried out in 1232 randomly chosen points scattered across farmers' plots. Crop types are shown for Galaba [Source: Mariotto et al., 2013].

Table 1. Hyperion images and Spectroradiometer data in two irrigated areas of 5 leading word crops. Three Hyperion hyperspectral images and several thousands of field ASD Spectroradiometer data were used to extract crop type information in the years 2006 and 2007 [Source: Mariotto et al., 2013]**.

| Satellite / Sensor | Number of images | Acquisition Dates | Crops |
|-----------------------|-------------------|--|---|
| Hyperion-EO1 | 3 | 29/5/2007 01/8/2007 06/8/2007 | Wheat, Cotton, Maize, Rice, and Alfalfa |
| ASD-Spectroradiometer | Several thousands | every 15-20 days May to Oct 2006 and 2007 | Wheat, Cotton, Maize, Rice, and Alfalfa |

*Original Hyperion images contain 242 bands, out of which 198 are calibrated and available in Google Earth

Engine. After removing problematic bands mostly affected by atmospheric noise, 158 bands were retained from 400 nm to 2500 nm.

**ASD Spectroradiometer wavelengths (1 nm) were averaged at 10 nm coincident to the band centers of the 158 Hyperion (10 nm width) selected bands.

IV. Algorithms description and data processing

Hyperion images were preprocessed in ENVI (Harris Geospatial Solutions, Inc.) and ArcGIS (ESRI) software. Hyperion digital numbers (DNs) were converted to absolute units of radiance ($W m^{-2} sr^{-1} \mu m^{-1}$), by splitting the VNIR and SWIR data into separate images because they were collected by two different spectrometers and thus had different calibration requirements (Scheffler and Karrasch, 2014, Datt et al. 2003, Bannari et al. 2015, Pervez et al. 2016). More recent approaches to processing hyperspectral data are discussed in Aneece and Thenkabail (2019a, 2019b) as well as in Aneece et al. (2018) and Aneece and Thenkabail (2018). Then, VNIR and SWIR digital numbers were converted to radiance by dividing digital numbers by 40 and 80 respectively (Barry 2001, Thenkabail et al. 2004, Thenkabail et al. 2013, Pervez et al. 2016). After recombining these datasets radiance was converted to apparent at-satellite reflectance (%) (Thenkabail, Enclona, Ashton, Legg, et al., 2004; Thenkabail, Enclona, Ashton, & VanDerMeer, 2004; Thenkabail et al., 2002, 2011), and finally to surface reflectance (%) after atmospheric correction (Figure 3). Atmospheric correction was performed using the Fast Line-of-sight Atmospheric Analysis of Spectral Hypercubes (FLAASH) tool in ENVI, which incorporates the MODTRAN4 radiation transfer code (Berk et al., 1999). All images were georectified and re-projected to a common UTM coordinate system and WGS84 datum in ArcGIS. Hyperion imagery consists of 242 contiguous spectral bands, of which only 198 are radiometrically calibrated (Beckmann & Mckinney, 2006). Among these 198 bands, 158 bands without any noise and free of atmospheric window effects were selected for this study. It must be noted that FLAASH was used in pre-processing in this effort since these data were processed earlier. Currently, we are using generic approaches to pre-processing by coding and computing on the cloud as described in Aneece and Thenkabail (2019a, 2019b) as well as in Aneece et al. (2018) and Aneece and Thenkabail (2018).

For the ASD Spectroradiometer wavelengths, 1 nm wide were measured every 10 nm coincident to the band centers of the 158 Hyperion (10 nm width) selected bands. Reflectance values of the pixels intersecting the ground data points were extracted from each satellite image for each band in ArcGIS.

The recently decommissioned hyperspectral satellite-borne sensor Hyperion collected over 70,000 images throughout the world, all of which are freely available through the USGS EarthExplorer and Google Earth Engine (GEE). These images can be used to build a spectral library of crops in different areas, years, and growth stages. Three Hyperion images and several thousands of ASD field spectroradiometer data measurements in Central Asia in 2006 and 2007 were used to map five globally dominant crops (maize, cotton, rice, wheat, and alfalfa).

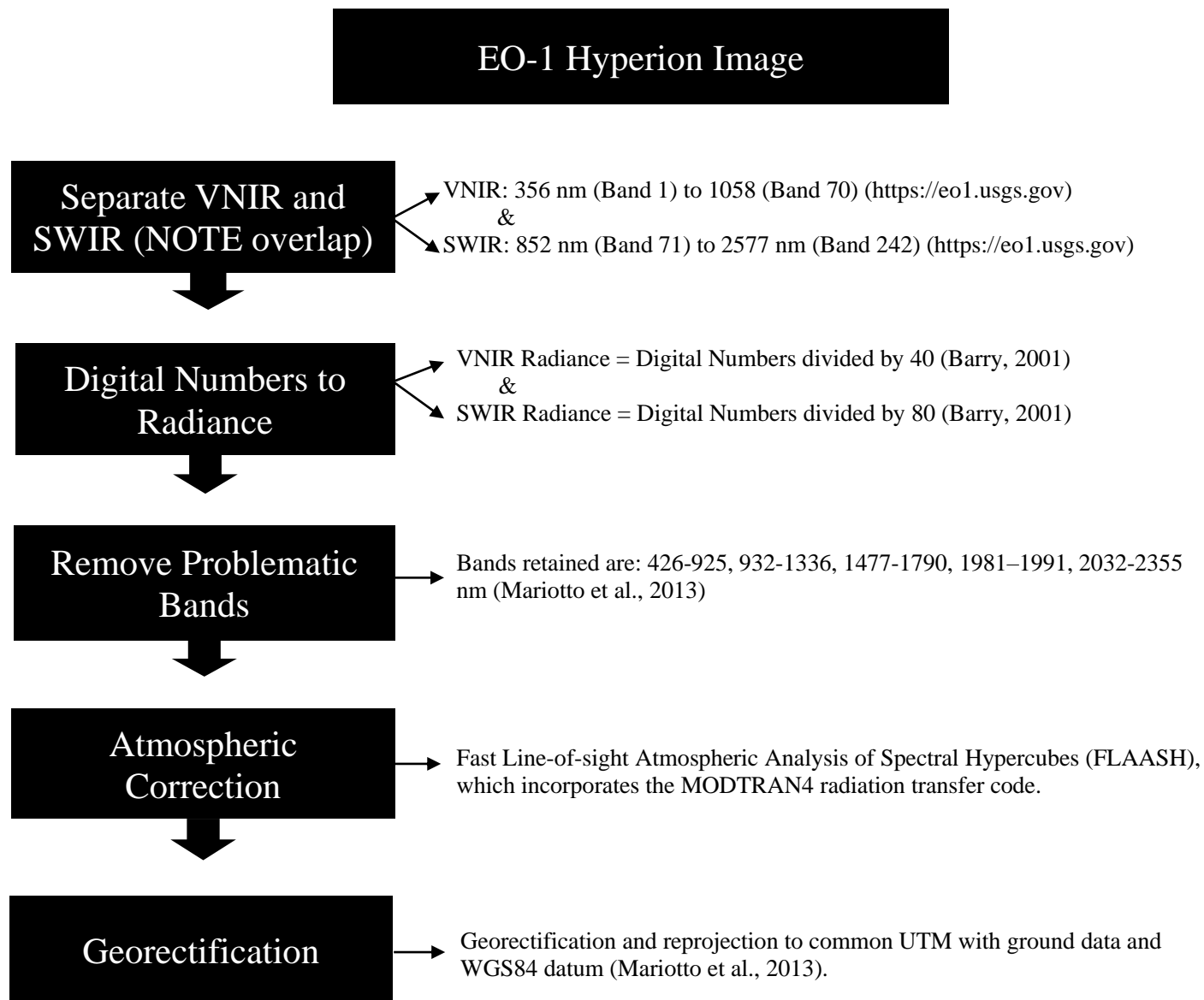


Figure 3. EO-1 Hyperion Pre-processing Workflow for GHISA Central Asia. [Source: Mariotto et al. 2013].

1. Algorithms

$$L = \left(\frac{A\rho}{1 - \rho_e S} \right) + \left(\frac{B\rho_e}{1 - \rho_e S} \right) + L_a \quad (1)$$

$$L_e \approx \left(\frac{(A + B)\rho_e}{1 - \rho_e S} \right) + L_a \quad (2)$$

S = spherical albedo of the atmosphere
A and B = atmospheric and geometric coefficients
 ρ_e = spatially averaged reflectance

1.1. Algorithm details

Algorithms for image pre-processing and spectral library (a.) and for selection of optimal wavebands to detect crop types (b.) are described below.

a. Image Pre-Processing and Spectral library

Hyperion images were preprocessed in ENVI and ArcGIS. FLAASH atmospheric correction was computed in ENVI. FLAASH incorporates the MODTRAN radiation transfer code. The spectral radiance at a sensor pixel, L (Equation 1), is calculated as the sum of the radiance reflected by each surface pixel (ρ) including correction (averaged value) for radiance scattering from surrounding pixels (ρ_e), that directly reaches the sensor and the radiance from surface that is scattered by the atmosphere into the sensor (L_a)

Then, wavelengths are recalibrated, and after water retrieval, pixel surface reflectances are calculated for all the sensor channels (Equation 2) by computing a spatially averaged radiance image L_e . This involves removing of cloudy pixels (Matthew et al., 2000).

Users can also select a MODTRAN aerosol/haze model and set visibility options to correct for presence of clouds, as well as apply spectral polishing for artifact suppression in hyperspectral data. More details are available in <https://www.harrisgeospatial.com/docs/FLAASH.html>

Crop spectra were extracted from pixels of Hyperion images with known crop types in ArcGIS. They can also be extracted in ENVI. These spectra were compiled into an Excel spreadsheet and problematic (noisy) bands were removed: 355-416 nm, 926-931 nm, 1346-1467 nm, 1800-1971 nm, 2002-2022, and 2365-2577 nm. Crop spectra from the ASD spectroradiometer are derived from data available in the Excel spreadsheet.

b. Algorithms for Selection of Optimal Wavebands to Detect Crop Types.

Algorithms for selection of optimal wavebands that detect the five leading crop types were developed in SAS (Statistical Analysis System, SAS Institute Inc.). Crop type discrimination was computed through the following statistical analyses for Hyperion and ASD Spectroradiometer data: (a) *Least square means* for assessing differences in band reflectance between three-, four-,

and five-crop types (wheat, cotton, maize, rice and alfalfa) by month. Pairwise comparisons of means were produced using the generalized linear model (GLM) procedure with the LSMEANS method in SAS. The tests were conducted for each month to see in which months the crops are best separated from each other, and which Hyperspectral Narrow Bands (HNBS) provided the best results.

(b) *Stepwise discriminant analysis* (STEPDISC procedure in SAS) using Wilk's lambda method (Wilks, 1935) is a powerful approach to select a subset of the wavebands that best separate crop types. The Wilk's lambda is the likelihood ratio criterion (ratio of within-group variance to the total variance) with a value ranging from 0 to 1: the higher the Wilk's lambda, the lesser the separability between crop types (0 means 100% separability of wheat, cotton, maize, rice, and alfalfa) (at significance level of $\alpha = 0.999$). Then, the Wilk's lambda values are plotted against the number of bands to determine the number of bands sufficient to best separate the 5 crops (when the curve becomes asymptotic or near-asymptotic) and their wavelength centers.

(c) *Principal component analysis (PCA)* (Pearson, 1901) establishes prominent bands most important for capturing highest variance in data, and helps eliminate data redundancy. The PCA was explored for each crop type separately to determine how best the characteristics of that crop are captured. The PCA was performed using the PRINCOMP procedure in SAS.

(d) *Correlation between narrowbands for determining optimal hyperspectral narrowbands*; to overcome the redundancy of HNBS, correlation between all combinations of narrowbands of Hyperion and spectroradiometer HNBS were conducted. The squared coefficients, R^2 , values were plotted in Lambda (λ_1) by Lambda (λ_2) plots to determine the HNB-centers and widths that provide the best and the redundant information.

(e) *Discriminant model and error matrices*: Finally, the most frequently occurring wavebands resulting from the LSmeans, Wilk's lambda, PCA, and lambda-lambda plots of hyperspectral Hyperion and Spectroradiometer data for the 5 leading crop types were analyzed through discriminant analysis (PROC DISCRIM in SAS), which resulted in error matrices (Congalton & Green, 2009).

The optimal band selection process is discussed in great detail by a series of recent book series by Thenkabail et al. (2018a,b,c,d) as well as in papers (Aneece and Thenkabail, 2018, Thenkabail et al., 2013, Mariotto and Thenkabail, 2013).

The resulting spectra, along with image information, geographic coordinates, crop type labels, and crop growth stage labels were compiled into the Global Hyperspectral Imaging Spectral-library of Agricultural crops (GHISA) for Central Asia.

1.2. Programming and code

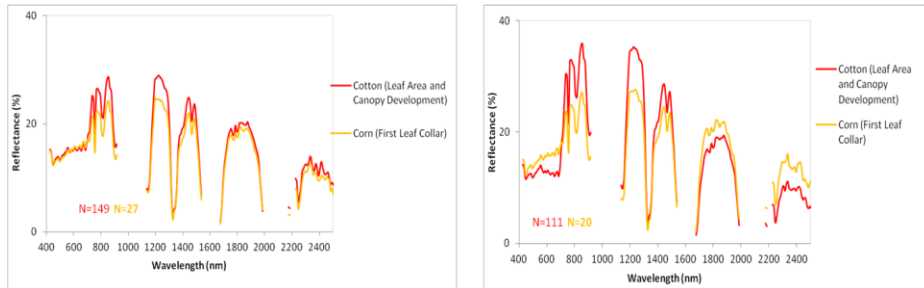
The Hyperion and ASD Spectroradiometer processing steps were coded in SAS. The codes are available for download along with this ATBD.

2. Results

a. Spectral Library

An illustration of the Hyperion hyperspectral profiles of cotton and corn in two different farms are reported in Figure 4. Illustration of Hyperion hyperspectral profiles of two cotton growth stages are shown in Figure 5 (a). Some spectroradiometer hyperspectral profiles of three growth stages of

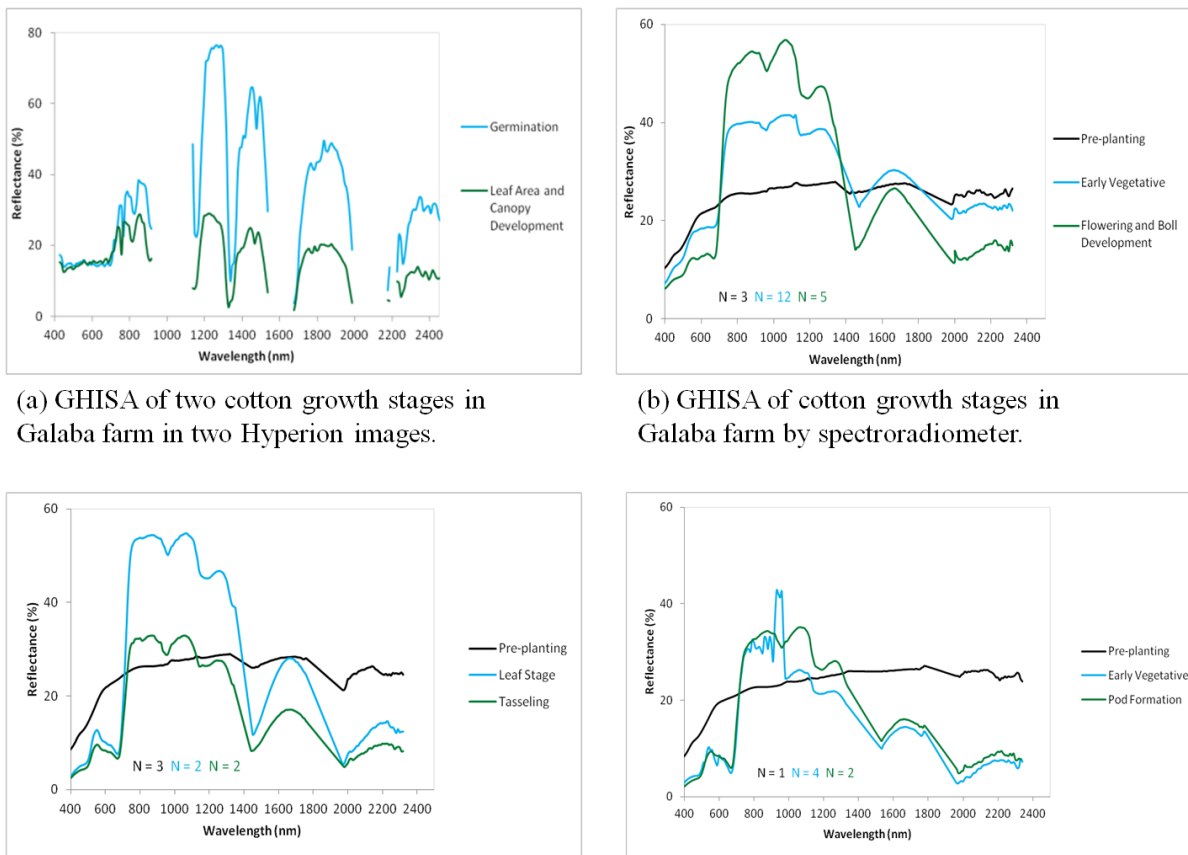
cotton, maize, and rice are shown in Figure 5. Data to derive all spectral profiles are in excel format and available to download.



(a) GHISA for cotton and corn in one Hyperion image (01 August) in Galaba farm.

(b) GHISA for cotton and corn in one Hyperion image (01 August) in Kuva farm.

Figure 4. Illustration of Global Hyperspectral Imaging Spectral library of Agricultural crops (GHISA) of Central Asia for two crops. N is number of spectra included in the average. [Source: Mariotto et al., 2013].



(a) GHISA of two cotton growth stages in Galaba farm in two Hyperion images.

(b) GHISA of cotton growth stages in Galaba farm by spectroradiometer.

(c) GHISA of corn growth stages in Galaba farm by spectroradiometer.

(d) GHISA of rice growth stages in Galaba farm by spectroradiometer.

Figure 5. Illustration of GHISA of Central Asia for three crops. GHISA illustrated for one crop in two growth stages (Hyperion) or three (ASD spectroradiometer) growth stages; and for three

growth stages for two other crops. N is number of spectra included in the average. [Source: Mariotto et al., 2013].

b. Algorithms for Selection of Optimal Wavebands that Detect Crop Types.

Algorithms for selecting best Hyperion and ASD spectroradiometer wavebands that detect the five leading crop types are derived from five statistical analyses:

- 1) *Least square means* has assessed differences in band reflectance between three-, four-, and five-crop types (wheat, cotton, maize, rice and alfalfa) by month are reported in Table 2;
- 2) *Stepwise discriminant analysis* of three crop types (cotton, maize, and wheat) has allowed selection of a subset of the wavebands that best discriminate crop types, and are reported at 99% confidence level in Figure 6;
- 3) *PCA* has selected the prominent bands that capture the highest variance in data for each crop type, and overcome data redundancy. The minimum set of unique bands (up to 5) computed through PCA that best explain the variability in reflectance across the different crop types are shown in Table 3;
- 4) *Correlation* between narrowbands, resulting in a total of 12,403 Pearson coefficients, has determined the optimal hyperspectral narrowbands and overcome data redundancy; and
- 5) *Discriminant model* has determined the final most frequently occurring wavebands (Figure 7) resulting from the above four statistical analyses. Its accuracies for both Hyperion and ASD Spectroradiometer in discriminating crop types are shown in Tables 4-6.

All the algorithms are in SAS format and are available to download.

Table 2. Least square means of crop types reflectance showing significant statistical discrimination power at 95% confidence level for Hyperion and ASD Spectroradiometer bands [Source: Mariotto et al., 2013]. Note: The data were collected during 2006 and 2007 growing seasons.

| | Cotton, Maize, Wheat Band centers (nm) | | | Cotton, Maize, Wheat, Rice Band centers (nm) |
|-------------------|---|---|---|--|
| | June | July | August | July |
| Hyperion | | | 437, 468-529, 569-712, 722, 752, 763, 875- 925, 933-1336, 1477-1498, 1790, 2073, 2093, 2103, 2123-2153, 2174, 2244, 2264, 2285, 2305-2355 | |
| Spectroradiometer | 581, 591 | 610-681, 702, 1441-1451, 1588-1740, 1961-2073, 2133-2194, 2214 | | 427-498, 610-681, 702 1441-1451, 1588-1740, 2081- 2193, 2214, 2244-2285 |

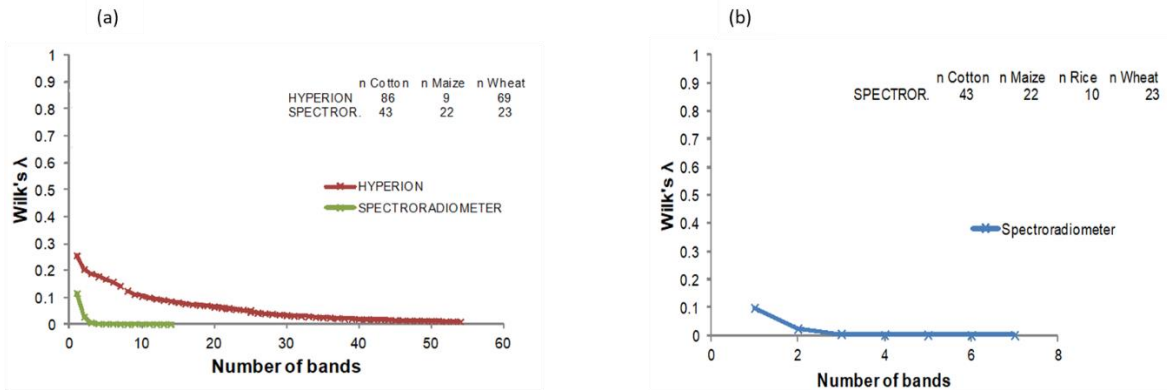


Figure 6. Crop type discrimination from Stepwise discriminant analysis: (a) Wilk's lambda separability of cotton, maize, and wheat for Hyperion and ASD Spectroradiometer; (b) Wilk's lambda separability of cotton, maize, and rice for spectroradiometer. **Note:** The lower the Wilk's Lambda, the greater the separability. n = number of pixels examined.

Table 3: The best Hyperion and ASD Spectroradiometer narrowband centers for the first five PCAs, selected on factor loadings (eigenvectors) for the five crop types.

| | | % Variability explained | | | | | | | | | | | | | |
|--------------------------|----------------|-------------------------|---------------|---------------|---------------|---------------|------|------|------|------|------|---------------------------|-----------------------------|----------------------------|----------------------------|
| | | PCA1 | PCA2 | PCA3 | PCA4 | PCA5 | PCA1 | PCA2 | PCA3 | PCA4 | PCA5 | First two cumulative PCAs | First three cumulative PCAs | First four cumulative PCAs | First five cumulative PCAs |
| | | b center (nm) | b center (nm) | b center (nm) | b center (nm) | b center (nm) | | | | | | | | | |
| HYPERION | Cotton | 1608 | 885 | 732 | 437 | 427 | 66 | 24 | 5 | 2 | 1 | 90 | 95 | 97 | 98 |
| | | 1588 | 875 | 712 | 963 | 732 | | | | | | | | | |
| | | 1568 | 824 | 722 | 1992 | 722 | | | | | | | | | |
| | | 1578 | 854 | 742 | 953 | 742 | | | | | | | | | |
| | | 1598 | 793 | 773 | 973 | 2042 | | | | | | | | | |
| | Maize | 722 | 1982 | 1124 | 943 | 1144 | 69 | 11 | 5 | 4 | 4 | 79 | 85 | 89 | 93 |
| | | 1558 | 1992 | 2335 | 933 | 1134 | | | | | | | | | |
| | | 1608 | 1488 | 933 | 1488 | 1982 | | | | | | | | | |
| | | 1638 | 2083 | 2204 | 2063 | 1992 | | | | | | | | | |
| | | 1679 | 2153 | 2244 | 2163 | 2264 | | | | | | | | | |
| | Wheat | 1568 | 1064 | 773 | 915 | 1134 | 66 | 27 | 2 | 0.9 | 0.6 | 93 | 96 | 97 | 98 |
| | | 1578 | 1104 | 752 | 885 | 1124 | | | | | | | | | |
| | | 1608 | 1084 | 763 | 895 | 1144 | | | | | | | | | |
| | | 1619 | 1094 | 783 | 864 | 1155 | | | | | | | | | |
| | | 1629 | 1054 | 793 | 875 | 963 | | | | | | | | | |
| SPECTRORADIOMETER | Alfalfa | 1769 | 1023 | 539 | 1790 | 681 | 48 | 45 | 5 | 1 | 0.6 | 93 | 98 | 99 | 99 |
| | | 2254 | 1003 | 549 | 2355 | 671 | | | | | | | | | |
| | | 1528 | 993 | 529 | 2335 | 661 | | | | | | | | | |
| | | 1518 | 1013 | 427 | 1780 | 691 | | | | | | | | | |
| | | 2224 | 963 | 559 | 1477 | 2073 | | | | | | | | | |
| | Cotton | 488 | 1669 | 640 | 447 | 2355 | 56 | 32 | 9 | 1 | 0.9 | 88 | 97 | 98 | 99 |
| | | 498 | 1679 | 702 | 549 | 2042 | | | | | | | | | |
| | | 478 | 1659 | 773 | 437 | 1982 | | | | | | | | | |
| | | 508 | 1649 | 661 | 427 | 2052 | | | | | | | | | |
| | | 559 | 1689 | 691 | 457 | 2073 | | | | | | | | | |
| | Maize | 681 | 1750 | 2355 | 2355 | 2305 | 54 | 40 | 2 | 1 | 0.7 | 94 | 97 | 98 | 99 |
| | | 671 | 1740 | 2345 | 2345 | 2335 | | | | | | | | | |
| | | 2042 | 1730 | 2335 | 1790 | 2315 | | | | | | | | | |
| | | 2032 | 1599 | 2325 | 2325 | 2224 | | | | | | | | | |
| | | 2052 | 1609 | 2295 | 549 | 2274 | | | | | | | | | |
| | Rice | 1528 | 915 | 712 | 722 | 712 | 57 | 40 | 2 | 0.6 | 0.4 | 97 | 99 | 99 | 100 |
| | | 1518 | 905 | 722 | 732 | 702 | | | | | | | | | |
| | | 1508 | 880 | 701 | 2325 | 590 | | | | | | | | | |
| | | 1538 | 885 | 549 | 712 | 2325 | | | | | | | | | |
| | | 1548 | 895 | 559 | 963 | 1074 | | | | | | | | | |
| | Wheat | 722 | 875 | 427 | 2345 | 2345 | 76 | 18 | 5 | 0.8 | 0.2 | 93 | 99 | 99 | 100 |
| | | 712 | 854 | 437 | 2355 | 2355 | | | | | | | | | |
| | | 1720 | 864 | 447 | 2315 | 712 | | | | | | | | | |
| | | 1709 | 834 | 457 | 2335 | 702 | | | | | | | | | |
| | | 1679 | 824 | 468 | 2325 | 722 | | | | | | | | | |

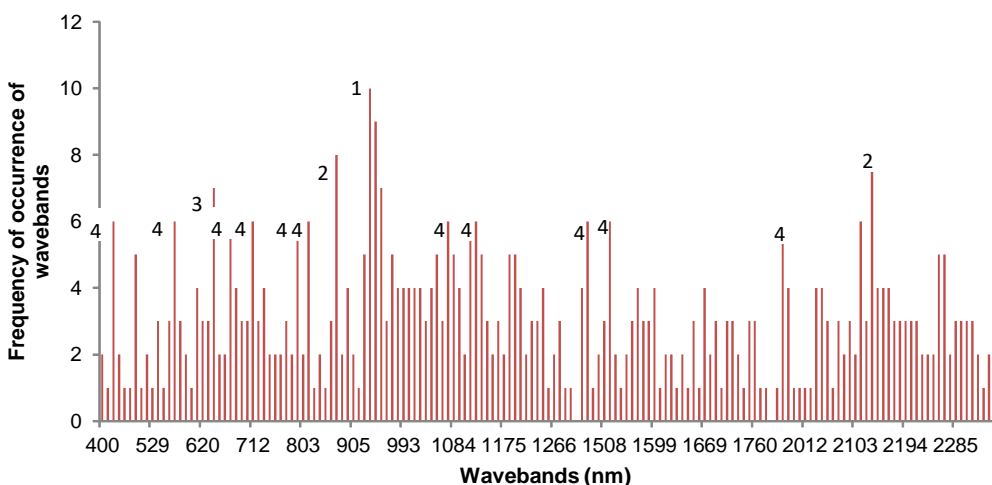


Figure 7. Frequency of occurrence of Hyperion narrowbands in LS-means, Wilk's lambda, PCA, and λ_1 - λ_2 R^2 . Groups of close narrowbands most frequently occurring (frequency ≥ 6) are ranked by progressive numbers above columns (1= most frequent).

Table 4. Overall accuracies, determined by discriminant model, of best Hyperion narrowbands in discriminating 3 crops: cotton, maize, and wheat. The wavebands were selected based on published research, now available in Thenkabail et al. (2018a,b,c,d).

| No. of bands | Waveband center (nm) | Overall Accuracy (%) |
|---|---|----------------------|
| <i>Three bands</i> NIR, FMIR | 885, 943, 2143 | 81.1 |
| <i>Five bands</i> blue, red, NIR, FMIR | 447, 651, 885, 943, 2143 | 82.3 |
| <i>Nine bands</i> VIS, Red edge, NIR, FMIR | 447, 579, 651, 681, 722, 803, 885, 943, 2143 | 83.5 |
| <i>Twelve bands</i> VIS, Red edge, NIR, FNIR, EMIR, FMIR | 447, 579, 651, 681, 722, 803, 885, 943, 1084, 1134, 1488, 2143 | 86 |
| <i>Fifteen bands</i> VIS, Red edge, NIR, FNIR, EMIR, FMIR | 447, 579, 651, 681, 722, 803, 885, 943, 1084, 1134, 1488, 1528, 1982, 2123, 2143 | 87.2 |
| <i>Twenty-nine bands</i> VIS, Red edge, NIR, MSNIR, FNIR, EMIR, FMIR | 447, 508, 579, 651, 681, 722, 803, 824, 885, 933, 943, 953, 963, 983, 1064, 1084, 1094, 1124, 1134, 1144, 1195, 1205, 1488, 1528, 1982, 2123, 2143, 2264, 2274 | 90.2 |

Table 5. Overall accuracies, determined by discriminant model, of best spectroradiometer narrowbands in discriminating 5 crops: alfalfa, cotton, maize, rice, and wheat. The wavebands were selected based reported research, now available in later edition (Thenkabail et al. 2018a,b,c,d).

| No. of bands | Waveband center (nm) | Overall Accuracy (%) |
|-------------------------------|----------------------|----------------------|
| <i>One band</i> blue | 437 | 71.2 |
| <i>Two bands</i> blue, red | 437, 681 | 75.7 |

| | | |
|--|--|------|
| <i>Four bands</i> blue, red, NIR, FMIR | 437, 681, 773, 1992 | 77.5 |
| <i>Seven bands</i> blue, red, NIR, FNIR, FMIR | 437, 681, 773, 1074, 1992, 2143, 2335 | 83.8 |
| <i>Eleven bands</i> blue, red, NIR, FNIR, EMIR, FMIR | 437, 681, 773, 1074, 1124, 1477, 1609, 1740, 1992, 2143, 2335 | 84.7 |
| <i>Twenty-one bands</i> blue, red, NIR, FNIR, EMIR, FMIR | 437 457 478 498 620 640 651 671 681 773 1074 1124 1477 1609 1740 19822 1992 2143 2335 | 92 |
| <i>Eighty bands</i> VIS, NIR, MSNIR, FNIR, EMIR, FMIR | 427 437 447 457 468 478 488 498 508 590 600 610 620 630 640 651 661 671 681 691 712 732 742 763 773 783 793 803 813 824 834 844 854 864 875 885 895 905 915 925 953 963 973 983 993 1003 1013 1033 1044 1054 1064 1084 1094 1104 1114 1124 1134 1144 1477 1599 1609 1659 1669 1679 1740 1750 1790 1982 1992 2032 2042 2052 2063 2073 2083 2103 2113 2123 2133 2335 | 93.7 |

Table 6. Classification accuracy matrix of 5 crops using best 21 spectroradiometer narrowbands (blue, red, NIR, FNIR, EMIR, FMIR)

| | Observed crop types | Classified crop types | | | | | Omission error % | Commission error % |
|----------------------------------|------------------------|-----------------------|--------------|------------|-----------|--------------|---------------------|-----------------------|
| | | Alfalfa | Cotton | Maize | Rice | Wheat | | |
| No. Classified crop type samples | Alfalfa | 13 | 0 | 0 | 0 | 0 | 0 | 0 |
| % Classified into crop type | | 100 | 0 | 0 | 0 | 0 | | |
| No. Classified crop type samples | Cotton | 0 | 42 | 1 | 0 | 0 | 2.3 | 0 |
| % Classified into crop type | | 0 | 97.67 | 2.33 | 0 | 0 | | |
| No. Classified crop type samples | Maize | 0 | 0 | 22 | 0 | 0 | 0 | 4.50 |
| % Classified into crop type | | 0 | 0 | 100 | 0 | 0 | | |
| No. Classified crop type samples | Rice | 0 | 0 | 0 | 3 | 7 | 70 | 10 |
| % Classified into crop type | | 0 | 0 | 0 | 30 | 70 | | |
| No. Classified crop type samples | Wheat | 0 | 0 | 0 | 1 | 22 | 4.3 | 30.4 |
| % Classified into crop type | | 0 | 0 | 0 | 4.35 | 95.65 | | |

V. Constraints and limitations

Constraints of the study included:

1. Limited availability of EO-1 Hyperion images during various growing periods;
2. Signal to noise ratio of EO-1 Hyperion data

VI. Conclusions

This is the first ever attempt to develop a comprehensive Global Hyperspectral Imaging Spectral-library of Agricultural Crops (GHISA). Three EO-1 Hyperion images in 2007 were analyzed along with several thousands of field ASD Spectroradiometer data collected in 2006 and 2007 were analyzed to develop GHISA hyperspectral libraries of agricultural crops of Central Asia. GHISA of Central Asia was developed for five major crops (corn, cotton, rice, alfalfa, and wheat). These hyperspectral libraries are made available for download through LP DAAC. Protocols for generating GHISA are available in this document. Other spectral libraries exist such as the USGS High Resolution Spectral Library (<https://www.usgs.gov/energy-and-minerals/mineral-resources-program/science/usgs-high-resolution-spectral-library>; <https://www.usgs.gov/labs/spec-lab>; Kokaly et al., 2017) that is focused on minerals, rocks, and soils, the ECOSTRESS Spectral Library 1.0 (<https://speclib.jpl.nasa.gov/>; Meerdink et al., 2019) that is focused on vegetation and non-photosynthetic vegetation, and the global vis-NIR soil spectral library (<http://www.sciencedirect.com/science/article/pii/S0012825216300113>; Rossel et al., 2019). This is the first, spectral library with overwhelming focus on agricultural crops of the world. Given the importance of agriculture for food and nutrition security of the global populations, this is an extremely important endeavor.

The goal of this effort is to build a comprehensive GHISA for the entire world using hyperspectral data from different platforms (e.g., spaceborne, airborne, drone-based, and ground-based) for the world's leading agricultural crops. The signature collection strategy allows for alternative collections by new instruments like German Aerospace Center's (DLR's) Earth Sensing Imaging Spectrometer (DESI) onboard International Space Station (ISS) or laboratory bench spectrometers or new generation of hyperspectral sensors such as India's HySIS (Hyperspectral Imaging Satellite) or upcoming new launches such as DLR's The Environmental Mapping and Analysis Program (EnMAP) from time to time. These are readily available now and provide technical advantages of scale and atmospherically pure signature development. We also want those who use spectra to try to transform spectra to various transformations to see whether those transformations such as, for example, first- or second-order derivative spectra provide greater uniqueness than regular spectra. In this specific effort, we developed GHISA for Central Asia based on EO-1 Hyperion and ASD spectroradiometer data. We will continue this effort for other parts of the world using other platforms in the future. The GHISA releases come with user guides, ATBDs, and the data processing code whether performed in GEE or otherwise.

VII. Publications

Mariotto, I., Thenkabail, P., Huete, A., Slonecker, T., and Platonov, A. 2013. Hyperspectral versus multispectral crop-productivity modeling and type discrimination for the HypsIRI mission. *Remote Sensing of Environment*, 139, 291–305. doi: 10.1016/j.rse.2013.08.002

Thenkabail, P., Mariotto, I., Gumma, M., Middleton, E., Landis, D., and Huemmrich, K. 2013. Selection of hyperspectral narrowbands (HNBS) and composition of hyperspectral two band vegetation indices (HVIs) for biophysical characterization and discrimination of crop types using field reflectance and Hyperion/ EO-1 data. *IEEE Journal of Selected Topics in Applied Earth Observations and Remote Sensing*, 6, 427–439.

VIII. Acknowledgements

This project was funded by the NASA ROSES HypsIRI research grant, NASA Science Mission Directorate's Earth Science Division. This project was funded by the United States Geological Survey (USGS). Support provided by the USGS Land Resources Mission Area (LRMA), and the National Land Imaging (NLI) and Land Change Science (LCS) programs are deeply appreciated.

IX. Contact information

LP DAAC User Services

U.S. Geological Survey (USGS)

Center for Earth Resources Observation and Science (EROS)

47914 252nd Street

Sioux Falls, SD 57198-0001

Phone Number: 605-594-6116

Toll Free: 866-573-3222 (866-LPE-DAAC)

Fax: 605-594-6963

Email: lpdaac@usgs.gov

Web: <https://lpdaac.usgs.gov>

For the Principal Investigators, feel free to write to:

Prasad S. Thenkabail at pthenkabail@usgs.gov

Isabella Mariotto at imariotto@terrasensinglab.com

Itiya Aneece at ianeece@usgs.gov

X. Citations

Mariotto, I., Thenkabail, P., and Aneece, I. 2020. Global Hyperspectral Imaging Spectral-library of Agricultural crops (GHISA) Area of Study: Central Asia. Algorithm Theoretical Basis Document (ATBD). NASA Land Processes Distributed Active Archive Center (LP DAAC). IP-116254. <https://doi.org/10.5067/Community/GHISA/GHISACASIA.001>

Mariotto, I., Thenkabail, P., and Aneece, I. 2020. Global Hyperspectral Imaging Spectral-library of Agricultural crops (GHISA) Area of Study: Central Asia. User Guide. NASA Land Processes Distributed Active Archive Center (LP DAAC). IP-116254. <https://doi.org/10.5067/Community/GHISA/GHISACASIA.001>

Mariotto, I., Thenkabail, P., Huete, A., Slonecker, T., and Platonov, A. 2013. Hyperspectral versus multispectral crop-productivity modeling and type discrimination for the HypsIRI mission. *Remote Sensing of Environment*, 139, 291–305. DOI: 10.1016/j.rse.2013.08.002

XI. References

Abdel-Rahman, E., Makori, D., Landmann, T., Piironen, R., Gasim, S., Pellikka, P., and Raina, S. 2015. The Utility of AISA Eagle Hyperspectral Data and Random Forest Classifier for Flower Mapping. *Remote Sensing*, 7, 13298-13318.

Adao, T., Hruska, J., Padua, L., Bessa, J., Peres, E., Morais, R., and Sousa, J. 2017. Hyperspectral Imaging: A Review on UAV-Based Sensors, Data Processing and Applications for Agriculture and Forestry. *Remote Sensing*, 9, 1110. Aneece, I. and Thenkabail, P. 2019a. Global Hyperspectral Imaging Spectral-library of Agricultural crops (GHISA) for the Conterminous United States (CONUS). Algorithm Theoretical Basis Document (ATBD). NASA Land Processes Distributed Active Archive Center (LP DAAC). IP-110217.

<https://lpdaac.usgs.gov/news/release-global-hyperspectral-imaging-spectral-library-agricultural-crops-conterminous-united-states/>

<https://lpdaac.usgs.gov/products/ghisaconusv001/>

Aneece, I. and Thenkabail, P. 2019b. Global Hyperspectral Imaging Spectral-library of Agricultural crops (GHISA) for the Conterminous United States (CONUS). User Guide. NASA Land Processes Distributed Active Archive Center (LP DAAC). IP-110217.

DOI: 10.5067/Community/GHISA/GHISAACONUS.001

<https://lpdaac.usgs.gov/news/release-global-hyperspectral-imaging-spectral-library-agricultural-crops-conterminous-united-states/> <https://lpdaac.usgs.gov/products/ghisaconusv001/>

Aneece, I. and Thenkabail, P. 2019. Global Hyperspectral Imaging Spectral-library of Agricultural crops (GHISA) for the Conterminous United States (CONUS). User Guide. NASA Land Processes Distributed Active Archive Center (LP DAAC). IP-110217.

DOI: 10.5067/Community/GHISA/GHISAACONUS.001

<https://lpdaac.usgs.gov/news/release-global-hyperspectral-imaging-spectral-library-agricultural-crops-conterminous-united-states/>

<https://lpdaac.usgs.gov/products/ghisaconusv001/>

Aneece, I.; Thenkabail, P. 2018. Accuracies Achieved in Classifying Five Leading World Crop Types and their Growth Stages Using Optimal Earth Observing-1 Hyperion Hyperspectral Narrowbands on Google Earth Engine. *Remote Sens.* 2018, 10, 2027. <https://doi.org/10.3390/rs10122027> IP-097093.

Aneece, I., and Thenkabail, P.S. 2018. Chapter 9 (of Volume I of Four-Volume Book): Spaceborne Hyperspectral EO-1 Hyperion Data Pre-Processing: Methods, Approaches, and Algorithms.

Volume I Title: Fundamentals, Sensor Systems, Spectral Libraries, and Data Mining for

Vegetation. Pp. 251-271. Book Title: “Hyperspectral Remote Sensing of Vegetation” (Second

Edition, 4 Volume Set). Publisher: CRC Press- Taylor and Francis group, Boca Raton, London, New York. Pp. 450. (Editors: Thenkabail, P.S., Lyon, G.J., and Huete, A.). IP-091722

Bannari, A., Staenz, K., Champagne, C., and Khurshid, K. 2015. Spatial variability mapping of crop residue using Hyperion (EO-1) hyperspectral data. *Remote Sensing*, 7, 8107–8127.

Barry, P., 2001. EO-1/ Hyperion Science Data User's Guide, Level 1 b. Pub. Release, L1 B HYP.TO.01.077, TRW Space, Defense and Information Systems, Redondo Beach, CA.

Bhattacharya, B., Green, R., Rao, S., Saxena, M., Sharma, S., Kumar, K., Srinivasulu, P., Sharma, S., Dhar, D., Bandyopadhyay, S., Bhatwadekar, S., and Kumar, R. 2019. An overview of AVIRIS-NG airborne hyperspectral science campaign over India. *Current Science*, 116 (7), 1082-1088. Biradar, C.M., Thenkabail, P.S., Noojipady, P., Yuanjie, L., Dheeravath, V., Velpuri, M., Turrall, H., Gumma, M.K., Reddy, O.G.P., Xueliang, L. C., Schull, M.A., Alankara, R.D., Gunasinghe, S., Mohideen, S., Xiao, X. 2009. A global map of rainfed cropland areas (GMRCAs) at the end of last millennium using remote sensing. *International Journal of Applied Earth Observation and Geoinformation*. 11(2). 114-129. [doi:10.1016/j.jag.2008.11.002](https://doi.org/10.1016/j.jag.2008.11.002). January, 2009.

Bracken, A., Coburn, C., Staenz, K., Rochdi, N., Segl, K., Chabrillat, S., and Schmid, T. 2019. Detecting soil erosion in semi-arid Mediterranean environments using simulated EnMAP data. *Geoderma*, 340, 164-174.

Buzzi, J., Riaza, A., Garcia-Melendez, E., Weide, S., and Bachmann, M. 2014. Mapping Changes in a Recovering Mine Site with Hyperspectral Airborne HyMap Imagery (Sotiel, SW Spain). *Minerals*, 4, 313-329.

Cahalane, C., Walsh, D., Magee, A., Mannion, S., Lewis, P., and McCarthy, T. 2017. Sensor Pods: Multi-Resolution Surveys from a Light Aircraft. *Inventions*, 2, 2, [doi:10.3390/inventions2010002](https://doi.org/10.3390/inventions2010002)

Chaube, N., Lele, N., Misra, A., Murthy, T., Manna, S., Hazra, S., Panda, M., and Samal, R. 2019. Mangrove species discrimination and health assessment using AVIRIS-NG hyperspectral data. *Current Science*, 116 (7), 1136-1142. Cai, X. Thenkabail, P. 2010. Using remote sensing to assess crop water productivity. SPIE Newsroom. DOI: 10.1117/2.1201002.002576. <http://spie.org/x39199.xml?highlight=x2420&ArticleID=x39199>.

Cai, X.L., Thenkabail, P.S., Biradar, C., Platonov, A., Gumma, M., Dheeravath, V., Cohen, Y., Goldshlager, N., Eyal Ben-Dor, Victor Alchanatis, and Vithanage, J.V. 2008. Water Productivity Mapping Methods and Protocols using Remote Sensing Data of Various Resolutions to Support “more crop per drop”. *Journal of Applied Remote Sensing*. 3(1) 033557 (2009); [doi:10.1117/1.3257643](https://doi.org/10.1117/1.3257643). Published October 12, 2009.

Clark, M. 2017. Comparison of simulated hyperspectral HypsIRI and multispectral Landsat 8 and Sentinel-2 imagery for multi-seasonal, regional land-cover mapping. *Remote Sensing of Environment*, 200, 311-325.

- Congalton, R. and Green, K., 2009. Assessing the accuracy of remotely sensed data: Principles and practices (2nd ed.). Boca Raton, FL: CRC/Taylor & Francis.
- Dao, P., He, Y., and Lu, B. 2019. Maximizing the quantitative utility of airborne hyperspectral imagery for studying plant physiology: An optimal sensor exposure setting procedure and empirical line method for atmospheric correction. *International Journal of Applied Earth Observation and Geoinformation*, 77, 140-150.
- Datt, B., McVicar, T., Van Niel, T., Jupp, D., and Pearlman, J. 2003. Preprocessing EO-1 Hyperion hyperspectral data to support the application of agricultural indexes. *IEEE Transactions on Geoscience and Remote Sensing*, 41, 1246–1259.
- Davidson, S., Santos, M., Sloan, V., Watts, J., Phoenix, G., Oechel, W., and Zona, D. 2016. Mapping Arctic tundra vegetation communities using field spectroscopy and multispectral satellite data in North Alaska, USA. *Remote Sensing*, 8, 978.
- Doneus, M., Verhoeven, G., Atzberger, C., Wess, M., and Rus, M. 2014. New ways to extract archaeological information from hyperspectral pixels. *Journal of Archaeological Science*, 52, 84-96.
- Franceschini, M., Bartholomeus, H., van Apeldoorn, D., Suomalainen, J., and Kooistra, L. 2017. Intercomparison of unmanned aerial vehicle and ground-based narrow band spectrometers applied to crop trait monitoring in organic potato production. *Sensors*, 17, 1428.
- Ghamisi, P., Yokoya, N., Li, J., Liao, W., Liu, S., Plaza, J., Rasti, B., and Plaza, A. 2017. Advances in hyperspectral image and signal processing: A comprehensive overview of the state of the art. *IEEE Geoscience and Remote Sensing Magazine*, DOI: 10.1109/MGRS.2017.2762087.
- Gumma, M., Thenkabail, P.S., Deevi, K., Mohammed, I., Teluguntla, P., Oliphant, A., Xiong, J., Aye, T., and Whitbread, A. 2018. Mapping cropland fallow areas in Myanmar to scale up sustainable intensification of pulse crops in the farming system. *GIScience & Remote Sensing*, 55 (6), 926-949.
- Guo, L., Zhang, H., Shi, T., Chen, Y., Jiang, Q., and Linderman, M. 2019. Prediction of soil organic carbon stock by laboratory spectral data and airborne hyperspectral images. *Geoderma*, 337, 32-41.
- Hoque, M. and Phinn, S. 2018. Chapter 12: Methods for linking drone and field hyperspectral data to satellite data. Volume I Title: Fundamentals, Sensor Systems, Spectral Libraries, and Data Mining for Vegetation. Pp. 321-354. Book Title: “Hyperspectral Remote Sensing of Vegetation” (Second Edition, 4 Volume Set). Publisher: CRC Press- Taylor and Francis group, Boca Raton, London, New York. Pp. 450. (Editors: Thenkabail, P.S., Lyon, G.J., and Huete, A.). (Editors: Thenkabail, P.S., Lyon, G.J., and Huete, A.). IP-091722. Available at: <https://www.routledge.com/Hyperspectral-Remote-Sensing-of-Vegetation-Second-Edition-FourVolume/Thenkabail-Lyon-Huete/p/book/9781138066250>

- Iqbal, A., Ullah, S., Khalid, N., Ahmad, W., Ahmad, I., Shafique, M., Hulley, G., Roberts, D., and Skidmore, A. 2018. Selection of HypsIRI optimal band positions for the earth compositional mapping using HyTES data. *Remote Sensing of Environment*, 206, 350-362.
- Ivushkin, K., Bartholomeus, H., Bregt, A., Pulatov, A., Franceschini, M., Kramer, H., van Loo, E., Roman, V., and Finkers, R. 2019. UAV based soil salinity assessment of cropland. *Geoderma*, 338, 502-512.
- Jha, C., Rakesh, Singhal, J., Reddy, C., Rajashekar, G., Maity, S., Patnaik, C., Das, A., Misra, A., Singh, C., Mohapatra, J., Krishnayya, N., Kiran, S., Townsend, P., and Martinez, M. 2019. Characterization of species diversity and forest health using AVIRIS-NG hyperspectral remote sensing data. *Current Science*, 116 (7), 1124-1135.
- Khurshid, K., Staenz, K., Sun, L., Neville, R., White, H., Bannari, A., Champagne, C., and Hitchcock, R. 2006. Preprocessing of EO-1 Hyperion data. *Canadian Journal of Remote Sensing*, 32 (2), 84-97.
- Kanning, M., Kühling, I., Trautz, D., Jarmer, T. 2018. High-Resolution UAV-Based Hyperspectral Imagery for LAI and Chlorophyll Estimations from Wheat for Yield Prediction. *Remote Sensing*, 10, 2000 doi: 10.3390/rs10122000
- Krutz, D., Muller, R., Knodt, U., Gunther, B., Walter, I., Sebastian, I., Sauberlich, T., Reulke, R., Carmona, E., Eckardt, A., Venus, H., Fischer, C., Zender, B., Arloth, S., Lieder, M., Neidhardt, M., Grote, U., Schrandt, F., Gelmi, S., and Wojtkowiak, A. 2019. The instrument design of the DLR Earth Sensing Imaging Spectrometer (DESI). *Sensors*, 19, 1622.
- Lausch, A., Salbach, C., Schmidt, A., Doktor, D., Merbach, I., and Pause, M. 2015. Deriving phenology of barley with imaging hyperspectral remote sensing. *Ecological Modelling*, 295, 123-135.
- Lee, C., Cable, M., Hook, S., Green, R., Ustin, S., Mandl, D., and Middleton, E. 2015. An introduction to the NASA Hyperspectral InfraRed Imager (HypsIRI) mission and preparatory activities. *Remote Sensing of Environment*, 167, 6-19.
- Legleiter, C., Overstreet, B., Glennie, C., Pan, Z., Fernandez-Diaz, J. and Singhanian, A. 2016. Evaluating the capabilities of the CASI hyperspectral imaging system and Aquarius bathymetric LiDAR for measuring channel morphology in two distinct river environments. *Earth Surface Processes and Landforms*, 41, 344-363.
- Lin, J., Pan, Y., Lyu, H., Zhu, X., Li, X., Dong, B., and Li, H. 2019. Developing a two-step algorithm to estimate the leaf area index of forests with complex structures based on CHRIS/PROBA data. *Forest Ecology and Management*, 441, 57-70.
- Maimaitiyiming, M., Miller, A. J., & Ghulam, A. 2016. Discriminating spectral signatures among and within two closely related grapevine species. *Photogrammetric Engineering & Remote Sensing*, 82(1), 51-62. doi: 10.14358/PERS.82.2.51
- Manfreda, S., McCabe, M., Miller, P., Lucas, R., Madrigal, V., Mallinis, G., Dor, E., Helman, D.,

- Estes, L., Ciruolo, G., Mullerova, J., Tauro, F., de Lima, M., de Lima, J., Maltese, A., Frances, F., Caylor, K., Kohv, M., Perks, M., Ruiz-Perez, G., Su, Z., Vico, G., and Toth, B. 2018. On the Use of Unmanned Aerial Systems for Environmental Monitoring. *Remote Sensing*, 10, 641.
- Mansour, K., Mutanga, O., Everson, T., and Adam, E. 2012. Discriminating indicator grass species for rangeland degradation assessment using hyperspectral data resampled to AISA Eagle resolution. *ISPRS Journal of Photogrammetry and Remote Sensing*, 70, 56-65.
- Mariotto, I., Thenkabail, P., Huete, A., Slonecker, T., and Platonov, A. 2013. Hyperspectral versus multispectral crop-productivity modeling and type discrimination for the HypsIRI mission. *Remote Sensing of Environment*, 139, 291–305. doi: 10.1016/j.rse.2013.08.002
- Marshall, M., and Thenkabail, P. 2014. Biomass modeling of four leading world crops using hyperspectral narrowbands in support of HypsIRI mission. *Photogrammetric Engineering & Remote Sensing*, 80, 757–772.
- Matsunaga T., Iwasaki, A., Tsuchida, S., Iwao, K., Tanii, J., Kashimura, O., Nakamura, R., Yamamoto, H., Kato, S., Obata, K., Mouri, K., Yamamoto, S., Tachikawa, T. 2018. Hisui Status Toward FY2019 Launch, IGARSS 2018 - 2018 IEEE International Geoscience and Remote Sensing Symposium, Valencia, pp. 160-163. doi: 10.1109/IGARSS.2018.8518639
- Matthew, M. W., S. M. Adler-Golden, A. Berk, S. C. Richtsmeier, R. Y. Levine, L. S. Bernstein, P. K. Acharya, G. P. Anderson, G. W. Felde, M. P. Hoke, A. Ratkowski, H.-H. Burke, R. D. Kaiser, and D. P. Miller, 2000. *Status of Atmospheric Correction Using a MODTRAN4-based Algorithm*. SPIE Proceedings, Algorithms for Multispectral, Hyperspectral, and Ultraspectral Imagery VI. Vol. 4049, pp. 199-207.
- Meij, B., Koositra, L., Suomalainen, J., Barel, J., Deyn, G. 2017. Remote sensing of plant trait responses to field-based plant–soil feedback using UAV-based optical sensors. *Biogeosciences*, 14, 733-749.
- Middleton, E. 2010. Diurnal and Directional Responses of Chlorophyll Fluorescence and the PRI in a Cornfield. 4th International Workshop on Remote Sensing of Vegetation Fluorescence, Valencia, Spain. Nov 15-17.
- Moharana, S. and Dutta, S. 2016. Spatial variability of chlorophyll and nitrogen content of rice from hyperspectral imagery. *ISPRS Journal of Photogrammetry and Remote Sensing*, 122, 17–29.
- Mourolis, P., Gorp, B., Green, R., Dierssen, H., Wilson, D., Eastwood, M., Boardman, J., Gao, B., Cohen, D., Franklin, B., Loya, F., Lundeen, S., Mazer, A., McCubbin, I., Randall, D., Richardson, B., Rodriguez, J., Sarture, C., Urquiza, E., Vargas, R., White, V., and Yee, K. 2014. Portable Remote Imaging Spectrometer coastal ocean sensor: design, characteristics, and first flight results. *Applied Optics*, 53 (7), 1363-1380.
- Mozgeris, G., Juodkiene, V., Jonikavicius, D., Straigyte, L., Gadal, S., and Ouerghemmi, W. 2018. Ultra-light aircraft-based hyperspectral and colour-infrared imaging to identify deciduous

- tree species in an urban environment. *Remote Sensing*, 10, 1668.
- Okujeni, A., Linden, S., and Hostert, P. 2015. Extending the vegetation–impervious–soil model using simulated EnMAP data and machine learning. *Remote Sensing of Environment*, 158, 69-80.
- Oliphant, A. J., Thenkabail, P. S., Teluguntla, P., Xiong, J., Gumma, M. K., Congalton, R. G., & Yadav, K. 2019. Mapping cropland extent of Southeast and Northeast Asia using multi-year time-series Landsat 30-m data using a random forest classifier on the Google Earth Engine Cloud. *International Journal of Applied Earth Observation and Geoinformation*, 81, 110-124.
- Ortenberg, F. 2018. Chapter 2: Hyperspectral sensor characteristics: Airborne, spaceborne, hand-held, and truck-mounted; Integration of hyperspectral data with LiDAR. Volume I Title: Fundamentals, Sensor Systems, Spectral Libraries, and Data Mining for Vegetation. Pp. 41-69. Book Title: “Hyperspectral Remote Sensing of Vegetation” (Second Edition, 4 Volume Set). Publisher: CRC Press- Taylor and Francis group, Boca Raton, London, New York. Pp. 450. (Editors: Thenkabail, P.S., Lyon, G.J., and Huete, A.). (Editors: Thenkabail, P.S., Lyon, G.J., and Huete, A.). IP-091722. Available at: <https://www.routledge.com/Hyperspectral-Remote-Sensing-of-Vegetation-Second-Edition-FourVolume/Thenkabail-Lyon-Huete/p/book/9781138066250>
- Oksouei, M. and Babakan, S. 2016. Detection of Alteration Minerals Using Hyperion Data Analysis in Lahroud. *Journal of the Indian Society of Remote Sensing*, 44(5), 713-721.
- Padghan, M., and Deshmukh, R. 2017. Spectroscopic determination of aboveground biomass in grass using partial least square regression model. *International Journal of Scientific Engineering and Technology*, 6 (9), 332-335.
- Panda, S. S., Rao, M.N., Thenkabail, P.S., Fitzgerald, J.E. 2015. Remote Sensing Systems – Platforms and Sensors: Aerial, Satellites, UAVs, Optical, Radar, and LiDAR, Chapter 1. In Thenkabail, P.S., (Editor-in-Chief), 2015. “Remote Sensing Handbook” (Volume I): Remotely sensed data characterization, classification, and accuracies. ISBN 9781482217865 - CAT# K22125. Taylor and Francis Inc.\CRC Press, Boca Raton, London, New York. Pp. 3-60. IP-060641.
- Pervez, W., Uddin, V., Khan, S., and Khan, J. 2016. Satellite-based land use mapping: Comparative analysis of Landsat-8, Advanced Land Imager, and big data Hyperion imagery. *Journal of Applied Remote Sensing*, 10, 026004-1–026004-20.
- Ratheesh, R., Chaudhury, N., Rajput, P., Arora, M., Gujrati, A., Arunkumar, S., Shetty, A., Baral, R., Patel, R., Joshi, D., Patel, H., Pathak, B., Jayappa, K., Samal, R., and Rajawat, A. 2019. Coastal sediment dynamics, ecology and detection of coral reef macroalgae from AVIRIS-NG. *Current Science*, 116 (7), 1157-1165.
- Rhee, D., Kim, Y., Kang, B., and Kim, D. 2018. Applications of unmanned aerial vehicles in fluvial remote sensing: An overview of recent achievements. *KSCE Journal of Civil Engineering*, 22 (2), 588-602.

- Riaza, A., Buzzi, J., Garcia-Melendez, E., Carrere, V., Sarmiento, A., and Muller, A. 2014. Monitoring acidic water in a polluted river with hyperspectral remote sensing (Hymap). *Hydrological Sciences Journal*, DOI: 10.1080/02626667.2014.899704
- Salem, S. 2017. ASD field hyperspectral measurements for discrimination of the ferruginous rocks and the iron ore types at El Gedida-Ghorabi area, Bahariya Oasis, Western Desert, Egypt. *Arabian Journal of Geosciences*, 10, 166.
- Scheffler, D., Karrasch, P., 2014. Destriping of hyperspectral image data: An evaluation of different algorithms using EO-1 Hyperion data. *Journal of Applied Remote Sensing*, 8, 083645–1 to 083645–18.
- Teluguntla, P., Thenkabail, P.S., Oliphant, A., Xiong, J., Gumma, M., Congalton, R., Yadav, K., and Huete, A. 2018. A 30-m Landsat-derived cropland extent product of Australia and China using random forest machine learning algorithm on Google Earth Engine cloud computing platform. *ISPRS Journal of Photogrammetry and Remote Sensing*, 144, 325-340.
- Thenkabail, P.S., Lyon, G.J., and Huete, A. (Editors) 2018a. Book Title: Hyperspectral Remote Sensing of Vegetation (Second Edition, Four Volume-set). Volume I Title: Fundamentals, Sensor Systems, Spectral Libraries, and Data Mining for Vegetation. Publisher: CRC Press-Taylor and Francis group, Boca Raton, London, New York. Pp. 449, Hardback ID: 9781138058545; eBook ID:9781315164151. <https://www.routledge.com/Fundamentals-Sensor-Systems-Spectral-Libraries-and-Data-Mining-for-Vegetation/Thenkabail-Lyon-Huete/p/book/9781138058545>
- Thenkabail, P.S., Lyon, G.J., and Huete, A. (Editors) 2018b. Book Title: Hyperspectral Remote Sensing of Vegetation (Second Edition, Four Volume-set). Volume II Title: Hyperspectral Indices and Image Classifications for Agriculture and Vegetation. Publisher: CRC Press- Taylor and Francis group, Boca Raton, London, New York. Pp. 296. Hardback ID: 9781138066038; eBook-ID:9781315159331. <https://www.routledge.com/Hyperspectral-Indices-and-Image-Classifications-for-Agriculture-and-Vegetation/Thenkabail-Lyon-Huete/p/book/9781138066038>
- Thenkabail, P.S., Lyon, G.J., and Huete, A. (Editors) 2018c. Book Title: Hyperspectral Remote Sensing of Vegetation (Second, Edition, Four-volume-set). Volume III Title: Biophysical and Biochemical Characterization and Plant Species Studies. Publisher: CRC Press- Taylor and Francis group, Boca Raton, London, New York. Pp. 348. Hardback: 9781138364714; eBook ID: 9780429431180 <https://www.routledge.com/Biophysical-and-Biochemical-Characterization-and-Plant-Species-Studies/Thenkabail-Lyon-Huete/p/book/9781138364714>
- Thenkabail, P.S., Lyon, G.J., and Huete, A. (Editors) 2018d. Book Title: Hyperspectral Remote Sensing of Vegetation (Second Edition, Four Volume-Set). Volume IV Title: Advanced Applications in Remote Sensing of Agricultural Crops and Natural Vegetation. Publisher: CRC Press- Taylor and Francis group, Boca Raton, London, New York. Pp. 386. Hardback: 9781138364769;-eBook-ID:9780429431166

<https://www.routledge.com/Advanced-Applications-in-Remote-Sensing-of-Agricultural-Crops-and-Natural/Thenkabail-Lyon-Huete/p/book/9781138364769>

- Thenkabail, P., Mariotto, I., Gumma, M., Middleton, E., Landis, D., and Huemmrich, K. 2013. Selection of hyperspectral narrowbands (HNBS) and composition of hyperspectral two band vegetation indices (HVIs) for biophysical characterization and discrimination of crop types using field reflectance and Hyperion/ EO-1 data. *IEEE Journal of Selected Topics in Applied Earth Observations and Remote Sensing*, 6, 427–439.
- Thenkabail, P.S. and Wu, Z. 2012. An Automated Cropland Classification Algorithm (ACCA) for Tajikistan by Combining Landsat, MODIS, and Secondary Data. *Remote Sensing*, 4, 2890-2918.
- Thenkabail, P.S., Hanjra, M., Dheeravath, V. and Gumma, M. 2010. A Holistic View of Global Croplands and Their Water Use for Ensuring Global Food Security in the 21st Century through Advanced Remote Sensing and Non-remote Sensing Approaches. *Remote Sensing*, 2, 211-261.
- Thenkabail, P., Enclona, E., Ashton, M., Legg, C., and de Dieu, M. 2014. Hyperion, IKONOS, ALI, and ETM+ sensors in the study of African rainforests. *Remote Sensing of Environment*, 90, 23–43.
- Thompson, D., Seidel, F., Gao, B., Gierach, M., Green, R., Kudela, R., and Mouroulis, P. 2015. Optimizing irradiance estimates for coastal and inland water imaging spectroscopy. *Geophysical Research Letters*, 42, doi:10.1002/2015GL063287.
- Verrelst, J., Romijn, E., and Kooistra, L. 2012. Mapping Vegetation Density in a Heterogeneous River Floodplain Ecosystem Using Pointable CHRIS/PROBA Data. *Remote Sensing*, 4, 2866-2889.
- Wilks, S. S., 1935. On the independence of k sets of normally distributed statistical variables. *Econometrika*, 3, 309 –326.
- Xu, Q., Liu, S., Ye, F., Zhang, Z., and Zhang, C. 2018. Application of CASI/SASI and fieldspec4 hyperspectral data in exploration of the Baiyanghe uranium deposit, Hebukesai, Xinjiang, NW China. *International Journal of Remote Sensing*, 39 (2), 453-469.
- Zhang, J., Rivard, B., Sanchez-Azofeifa, A., and Castro-Esau, K. 2006. Intra- and inter-class spectral variability of tropical tree species at La Selva, Costa Rica: Implications for species identification using HYDICE imagery. *Remote Sensing of Environment*, 105, 129-141.